 doi:10.20944/preprints202108.0499.v1

Type of the Paper (Article, Review, Communication, etc.)

Analysis of Local and Global Aromaticity in Si_3C_5 and Si_4C_8 Clusters. Aromatic Species Containing Planar Tetracoordinate Carbon

Juan Torres-Vega,[1] Diego R. Alcoba,[2,3] Ofelia B. Oña,[4] Alejandro Vásquez-Espinal,[5] Rodrigo Báez-Grez,[5] Luis Lain,[6] Alicia Torre,[6] Victor Garcia*[7] and William Tiznado*[5]

1 Centro de Investigaciones Tecnológicas, Biomédicas y Medioambientales, Calle José Santos Chocano 199, Urb. San Joaquín, Callao, Perú.
2 Departamento de Física, Facultad de Ciencias Exactas y Naturales, Universidad de Buenos Aires, Ciudad Universitaria, 1428 Buenos Aires, Argentina.
3 Instituto de Física de Buenos Aires, Consejo Nacional de Investigaciones Científicas y Técnicas, Ciudad Universitaria, 1428 Buenos Aires, Argentina.
4 Instituto de Investigaciones Fisicoquímicas Teóricas y Aplicadas, Universidad Nacional de La Plata, CCT La Plata, Consejo Nacional de Investigaciones Científicas y Técnicas. Diag. 113 y 64 (S/N), Sucursal 4, CC 16, 1900 La Plata, Argentina.
5 Computational and Theoretical Chemistry Group, Departamento de Ciencias Químicas, Facultad de Ciencias Exactas, Universidad Andres Bello, República 498, Santiago, Chile.
6 Departamento de Química Física, Facultad de Ciencia y Tecnología, Universidad del País Vasco. Apdo. 644, E-48080 Bilbao, Spain.
7 Departamento Académico de Fisicoquímica - Facultad de Química e Ingeniería Química, Universidad Nacional Mayor de San Marcos, Lima, Perú.

* Correspondence: victor.garcia@unmsm.edu.pe (V.G.) and wtiznado@unab.cl (W.T.)

Abstract: The minimum energy structures of the Si_3C_5 and Si_4C_8 clusters are planar and contain planar tetracoordinate carbons (ptCs). These species have been classified, qualitatively, as global (π) and local (σ) aromatics according to the adaptive natural density partitioning (AdNDP) method, which is an orbital localization method. This work evaluates these species' aromaticity, focusing on confirming and quantifying their global and local aromatic character. For this purpose, we use an orbital localization method based on the partitioning of the molecular space according to the topology of the electronic localization function (LOC-ELF). In addition, the magnetically induced current density is analyzed. The LOC-ELF-based analysis coincides with the AdNDP study (double aromaticity, global and local). Besides, the current density analysis detects global and local ring currents. The strength of the global and local current circuit is significant, involving 4n+2 π- and σ-electrons, respectively. The latter implicates the Si-ptC-Si fragment, which would be related to the 3c-2e σ-bond detected by the orbital localization methods in this fragment.

Keywords: Clusters; planar tetracoordinate carbon (ptC); local and global aromaticity; chemical bonding; orbital localization; electron localization function (ELF); electron delocalization; current density analysis.

1. Introduction

The concept of aromaticity has been extended over time to coin new features that define a system as aromatic and address a diversity of organic and inorganic systems [1–5]. In this regard, nowadays, the concept of aromaticity, π, and σ, is extensively used to rationalize the stability of some atomic clusters [6]. Accordingly, the aromaticity well justifies the clusters' highly symmetric and stable structures. So, numerous planar boron clusters [7–9], metal clusters [1,5–7,10–14], and metallabenzenes [15–19] fit well into the

Preprints (www.preprints.org) | NOT PEER-REVIEWED | Posted: 25 August 2021 doi:10.20944/preprints202108.0499.v1

concept of aromaticity. Along with π- and σ-aromaticity, multiple local π-aromaticity shows to be a helpful concept for rationalizing complex conjugate systems such as polycyclic hydrocarbons or graphene [20,21]. Moreover, it was indicated that the concept of multiple local σ-aromaticity is also applicable in the chemistry of nonagermanide clusters [22].

Chemists dedicate considerable effort to predict new molecules with exotic non-classical structures. Planar hypercoordinate carbons, i.e., carbon linked to four or more ligands in the plane, are especially puzzling systems. With the modest goal of achieving a thermally accessible transition state for a classical racemization experiment, in 1970, Hoffman and coworkers introduced strategies to stabilize a planar tetracoordinate carbon (ptC) [23]. Notably, this study inspired many theoretical and experimental studies over the last 50 years culminating in numerous compounds with ptC's [24–30]. More recently, "planar hypercoordinate" chemistry expanded to include planar species where the central atom is not limited to carbon, and the coordination number is more than four. Species with planar pentacoordinate [31–39] and hexacoordinate [40–43] carbons (ppC's or phC's) have been designed *in silico*. Electronic delocalization (i.e., aromaticity, resonance) plays a determining role in the stability of many of these species. Consequently, the comprehensible chemical bonding analysis is fundamental for interpreting their stability. For instance, the 18-valence electron D_{4h}-CAl_4^{2-} cluster is a doubly σ- and π-aromatic cluster experimentally detected in the $Na^+[CAl_4^{2-}]$ complex [29,30]. Of particular interest in this work is the concept of aromaticity (π, σ, local, global) and the role it plays in justifying the stability of systems with planar hypercoordinate carbons.

Aromaticity is not an observable property, yet it is generally assessed in terms of structural, energetic, and magnetic criteria [3,44–49]. Aromatic and antiaromatic species sustain diatropic and paratropic ring current when exposed to a uniform magnetic field perpendicular to the molecular plane [50–55]. This magnetic response allows to interpret experimental NMR spectroscopy and magnetic anisotropy measurements on (anti) aromatic molecules [46,56]. The nucleus-independent chemical shifts (NICS) is a very popular theoretical descriptor used for assessing aromaticity. Schleyer and coworkers defined NICS as "the negative of the absolute magnetic shielding," further suggesting to compute it at the molecular center [57]. Note that Biot–Savart law connects the induced magnetic field at the ring center, and thus the chemical shift at this point, to the ring current density [58]. In particular, the out-of-plane component of the NICS measured above the molecular plane [i.e., $NICS_{zz}(1)$] is well correlated with the intensity of the ring current flux (according to ring current strength, RCS, values) [59,60]. However, some works reported significant discrepancies between NICS-based and current density-based analyses for systems with multiple (local and global) aromaticity (i-e. aromatic polycyclic hydrocarbons) [61,62]. This is because the NICS is affected by coupling contributions from local and global aromatic circuits, blurring the inferences of local, semilocal, and global ring currents in these systems.

Previously, some of the authors of this work had designed a series of ptC global minima composed of carbon and heavier atoms of group 14 of the periodic table [63–65]. The design strategy consisted of replacing three consecutive protons from an aromatic hydrocarbon by one E_2^{4+} fragment (E=Si-Pb), favoring the preservation of the π-aromatic circuits of the parent aromatic hydrocarbons (see Scheme 1) [63]. Interestingly, the systems Si_3C_5, Ge_3C_5, Si_4C_8 and Ge_4C_8 ($C_5H_5^-$ and $C_8H_6^{2-}$ derivatives) contain one or two ptCs in their lowest energy structures. The chemical bonding analysis –employing the adaptive natural density partitioning analysis (AdNDP)– suggests that these systems are globally π-aromatic and locally σ-aromatic. This aromatic character was supported by the analysis of the nucleus independent chemical shift (NICS).

Preprints (www.preprints.org) | NOT PEER-REVIEWED | Posted: 25 August 2021 doi:10.20944/preprints202108.0499.v1

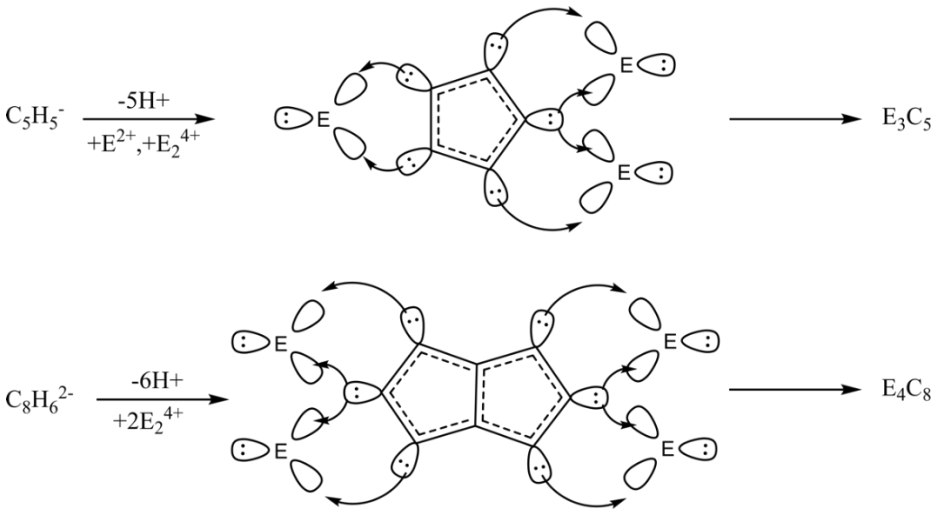

Scheme 1. Design strategy of aromatic ptC systems employed in reference [63].

Given the NICS problems mentioned above, we analyze the local and global ring currents in the Si_3C_5 and Si_4C_8 systems in this work. In addition, we have analyzed the chemical bonding with the ELF-LOC method, an orbital localization scheme in the domains of the electronic localization function (ELF). ELF-LOC, like AdNDP, provides information related to electronic delocalization. Our results confirm the presence of two delocalization circuits, one global (π) and one local (σ). More importantly, the global and local ring currents are diatropic and significant (according to ring current strength, RCS, calculations). These results strongly support these systems' double aromatic character (local and global) and their role in their stability.

2. Materials and Methods

Geometry optimizations were performed at B3LYP [66]/6-311+G* [67,68] level. Vibrational frequencies were evaluated at the same level to confirm the optimized structures as true minima on their potential energy surface using Gaussian16 program [69]. Cartesian coordinates of the optimized structures are shown in Table S1.

A detailed description of the ELF-LOC algorithm can be found elsewhere [70–73]. In this work, all numerical determinations were performed at the B3LYP level within density functional theory (DFT), using the atomic STO-3G basis sets. The overlap integrals over ELF regions, required to calculate the localized natural orbitals, have been obtained from the GAMESS computational package [74] and a modified version of the ToPMoD program [75]. The orbital localization has been performed using our codes [70,71].

NICS were computed using the gauge-including atomic orbital (GIAO) [76] method and dissected into their core, σ and π contributions, using the natural chemical shielding (NCS) [77] analysis as implemented in the NBO 6.0 program [78]. To evaluate NICS, we used NICSall, a simple program developed in our group, which is interfaced with the Gaussian program. NICSall helps to prepare the inputs and submits the calculations to generate the data according to the user's requirements. In this work, we computed NICS in 2D. To do this, we first estimated the box size; which in this case has been defined by the sides equal to 1.5 times the length and width of the molecule (centered and placed in the XY plane); by the height (z-axis), taking their lowest value. NICSall prepares the inputs to fill the grid with a step size of 0.2 Å (this is a default value; it could be modified by the user). Finally, NICSall delivers the outputs: text files with the properties (scans, FiPC-NICS) or cube files to plot maps and isosurfaces. The NICS plots were performed with the VisIt 3.0.2 program [79].

Current densities were computed with the GIMIC program [80,81] using the gauge including the atomic orbital (GIAO) [76] method. In the calculations, the magnetic field is directed along the z-axis, i.e., perpendicular to the molecular plane. The unit for current

Preprints (www.preprints.org) | NOT PEER-REVIEWED | Posted: 25 August 2021 doi:10.20944/preprints202108.0499.v1

susceptibility is nA T^{-1} and the results are, therefore, independent of the magnitude of the magnetic field. For a qualitative analysis, vector plots of the current density in a plane placed 0.0, and 0.5 Å above the molecular plane, were generated. Diatropic (aromatic) and paratropic (antiaromatic) currents are assumed to circle clockwise and counterclockwise, respectively. Current pathways are visualized using Paraview [82,83]. Ring current strengths (RCS), a measure of the net current intensity around the molecular ring, were obtained after considering different integration planes (see Figures S1-S3). The integration planes correspond to cut-off planes perpendicular to the chosen bonds of the molecule and extend horizontally along the ring's plane in 3.8/3.6 Å for 6C/5C ring members, respectively and, with 2.6 Å above and below the ring. The two-dimensional Gauss-Lobatto algorithm [81,84] was used to integrate the current passing through an integration plane.

Vector plot visualization of the current density in the plane of the molecule and 0.5Å above are reported in Figures S1-S5. It is essential to mention that negative (diatropic) and positive (paratropic) NICS at the center of the molecules are associated with aromaticity and anti-aromaticity. In contrast, for RCS, a positive (diatropic) and negative (paratropic) sign correspond to aromatic and anti-aromatic molecules, respectively. For both NICS and RCS, values close to zero suggest non-aromatic behavior [85]. Both, NICS and current density analysis were performed at B3LYP/6-311+G* level.

We performed Geometry optimizations and vibrational modes computations at B3LYP [66]6-311+G* [67,68] level, the latter to verify that structures correspond to true minima over the potential energy surface, using the Gaussian16 program [69]. Table S1 shows the Cartesian coordinates of the optimized systems.

A detailed description of the ELF-LOC methodology is given in references [70–73]. For this work, we used the wave function at the B3LYP/STO-3G level in the optimized geometries at the B3LYP/6-311+G* level. We used the computational package GAMESS [74], a modified version of the ToPMoD program [75], and our codes [70,71] to obtain the ELF-LOC localized orbitals.

We computed NICS using the gauge included atomic orbitals (GIAO) method [76] and dissected into their σ and π contributions using natural chemical shielding (NCS) analysis [77] implemented in the NBO 6.0 program [78]. For the easy computation of NICS, we used the NICSall tool (interfaced with Gaussian program), a simple pipeline developed in our group. In this work, we compute NICS in two dimensions (2D). The molecule was placed in the XY plane and centered at the origin of coordinates. Thus, we defined the width (1.5 times the length of the molecule) and location of the plane (in the molecular plane and perpendicular to the molecular plane). NICSall generated inputs to fill the mesh with a step size of 0.2 Å. We plotted NICS values on the planes with the VisIt 3.0.2 program [79].

Current densities were calculated with the GIMIC program [80,81] using the gauge method, including the atomic orbital (GIAO) [76]. The external magnetic field is directed perpendicular to the molecular plane (Z-axis) in the calculations. The unit for the current strength is nA T-1, so the results are independent of the magnitude of the external magnetic field. For qualitative analysis, we built vector plots of the current density on defined planes. By convention (in these calculations), diatropic (aromatic) and paratropic (antiaromatic) currents flow clockwise and counterclockwise, respectively. We used the Paraview program [82,83] to generate the current density vectors plots. The ring current strengths (RCS), a measure of the net current strength around the molecular ring, were obtained after considering different integration planes (see Figures S1-S3). The integration planes extend horizontally along the ring plane by 3.8/3.6 Å for the 6C/5C ring members, respectively, and 2.6 Å above and below the ring. GIMIC uses the two-dimensional Gauss-Lobatto algorithm [81,84] to integrate the current passing through an integration plane.

The location of the integration planes is shown in Figures S1-S5. It is essential to clarify that negative (diatropic) and positive (paratropic) NICS values at the center of the molecules are associated with aromaticity and antiaromaticity, respectively. On the contrary, in RCSs, a positive (diatropic) and negative (paratropic) sign correspond to aromatic and

Preprints (www.preprints.org) | NOT PEER-REVIEWED | Posted: 25 August 2021 doi:10.20944/preprints202108.0499.v1

antiaromatic molecules, respectively. In both NICS and RCS, values close to zero suggest an absence of aromaticity [85]. Both NICS and current density analysis were performed at the B3LYP/6-311+G* level.

3. Results

For the sake of clarity, our analysis will be divided into two parts: the chemical bonding analysis according to the ELF-LOC method and the global and local aromaticity analysis according to magnetic criteria.

3.1. Chemical Bonding Analisis according to ELF-LOC method.

The orbital localization provided by the ELF-LOC method reveals a chemical bonding pattern similar to that described by AdNDP. In Si_3C_5 and Si_4C_8, the C_5 and C_8 rings are connected by 2-center two-electron C-C σ-bonds (2c-2e). For Si_4C_8, one C-C σ-bond (2c-2e) that splits the C_8 ring into two pentagons is also detected. Additionally, delocalized bonds are detected, three π-bonds in the case of Si_3C_5 and five in Si_4C_8. Note that in this set, the π-orbitals are distributed over the entire molecular structure. Besides, delocalized σ-bonds (3c-2e) are also detected in each Si-ptC-Si triangular fragment. These results support global π- and local σ-delocalization, suggesting possible global and local aromaticity according to Hückel's 4n+2 rule [86–88].

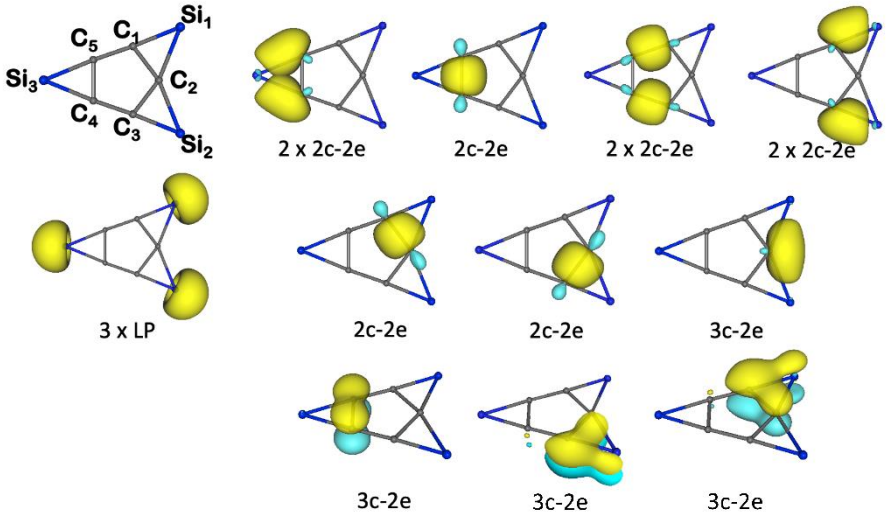

Figure 1. Results of ELF-LOC for Si_3C_5 cluster.

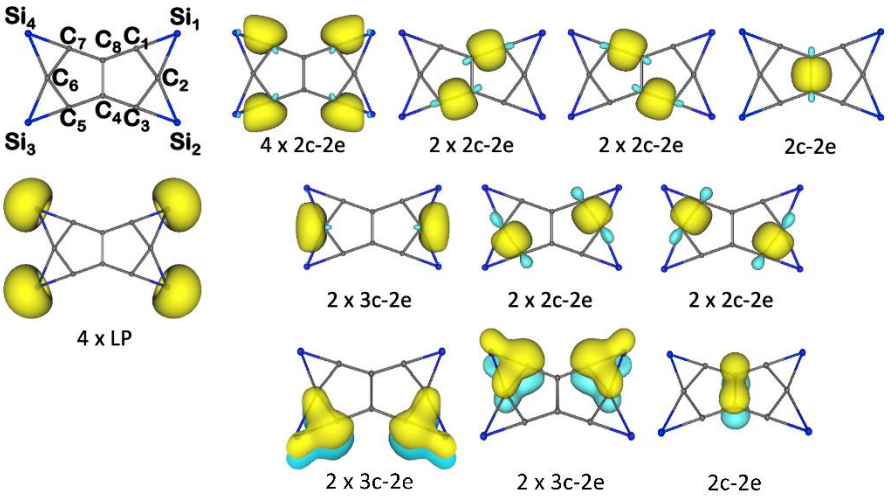

Figure 2. Results of ELF-LOC for Si_4C_8 cluster.

Preprints (www.preprints.org) | NOT PEER-REVIEWED | Posted: 25 August 2021 doi:10.20944/preprints202108.0499.v1

3.2. Current Density Analysis.

According to the magnetic criteria, in the presence of an external magnetic field, aromatic (antiaromatic) molecules sustain diatropic (paratropic) currents. In contrast, in nonaromatic molecules, the currents in one direction or the other cancel out, giving a resultant current strength close to zero [54–56,81,85,89,90]. In this work, we define as "local ring current" the current circuits distributed in a local molecular ring. In contrast, we describe the "global ring current" circuit distributed around the whole molecule. This assignment was introduced by Sundholm et al. [62] and recently used by our group to highlight the shortcomings of NICS in assessing the aromaticity of polycyclic systems [91]. Note that Aihara introduced a similar concept to distinguish between different current density pathways [92].

We can glimpse the patterns of current flows by inspecting current density plots. Hence, the magnetically induced current density of Si_3C_5 and Si_4C_8 systems, calculated in a plane located 0.5 Å above the molecular plane, are shown in Figures 3 and 4 (part a). These plots will guide our selection of the integration planes. The different contributions (bond, atomic and ring currents) are defined and quantified by analyzing the integration profiles along the integration planes, see Figures S1-S2. In this way, it is possible to computationally determine the local and global character of the induced currents. The strength of the local currents (diatropic) is computed and, then subtracted from the strength of the diatropic current connecting the local rings to determine the global RCSs [62,91]. Accordingly, it has been possible to identify the different delocalization circuits in the studied systems (part b of Figures 3 and 4). In addition, the intensity of each current is also shown in these figures. For the Si_3C_5 system, an intense and paratropic current is detected inside the C_5 (RCS= -8.06 nA/T). This ring current is more paratropic than that exhibit by the cyclopentadienyl anion (-3.5 nA T^{-1}), the results of which are shown in Figure S3. A global diatropic ring current with a strength of 12.2 nA T^{-1} is also detected. The latter result from the delocalization of the six π-electrons and is weaker than that of the cyclopentadienyl anion (14.5 nA T^{-1}). The differences may be due to the effect of the polarization of the π-electron cloud toward the silicon atoms. This hypothesis is supported by analyzing the $Si_2C_5H_2$ system, with one less bridged silicon atom exhibiting a paratropic (RCS=-3.6 nA T^{-1}) and diatropic (RCS=13.4 nA T^{-1}) current intensity closer to those of the cyclopentadienyl anion (see Figures S3 and S5). Interestingly, a local diatropic ring current involving the Si-ptC-Si fragment is also detected, in complete agreement with that predicted by AdNDP and ELF-LOC, which indicated the presence of a σ-delocalized 3c-2e bond. Moreover, the RCS value (5.2 nA/T) suggests that this species has a moderate local σ-aromatic character.

For the case of the Si_4C_8 system (Figure 4), the current density analysis detects two paratropic and local ring currents (within each C_5 ring). Similar to Si_3C_5, these currents are more paratropic (RCS=-4.7 nA T^{-1}) than those of the pentalene dianion (RCS=-4.4 nA T^{-1}), whose current density analysis is shown in Figure S4. We also detect a weak global paratropic ring current (RCS=-1.6 nA T^{-1}) distributed around C_8 fragment in addition to an intense global diatropic current (RCS=10.4 A T^{-1}). The global diatropic current is less intense than those of the pentalene dianion (RCS=10.4 A T^{-1}), presumably because of the polarization of the π-electron cloud toward the silicon. Finally, two local sigma currents are detected, involving the Si-ptC-Si circuits, similar to that exhibit by Si_3C_5 system. Moreover, these currents are of moderate intensity (RCS=5.8 nA T^{-1}) leaving in evidence the local sigma aromatic character of these species.

Preprints (www.preprints.org) | NOT PEER-REVIEWED | Posted: 25 August 2021 doi:10.20944/preprints202108.0499.v1

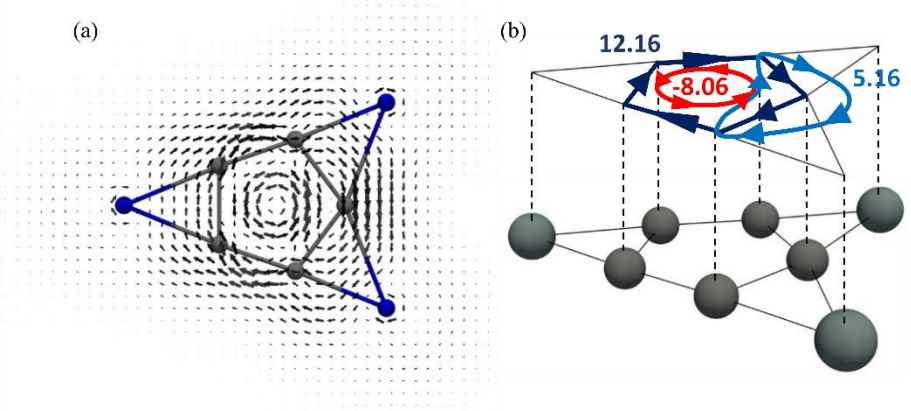

Figure 3. (a) Vector plot visualization of the current density of Si_3C_5 in a plane placed 0.5 Å above the molecular plane; (b) Schematic representation of local and global currents.

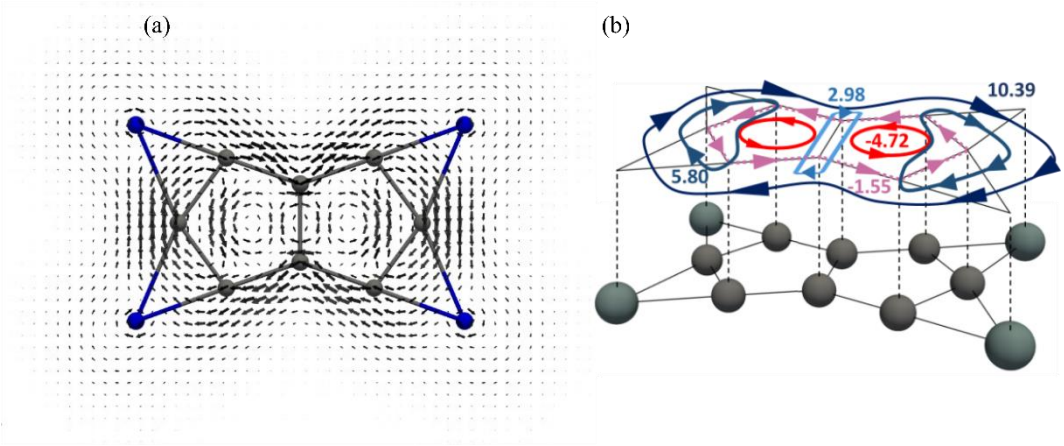

Figure 4. (a) Vector plot visualization of the current density of Si_4C_8 in a plane placed 0.5 Å above the molecular plane; (b) Schematic representation of local and global currents.

3.2. NICS Analysis.

Figure 5 shows the σ and π-components of the $NICS_{zz}$ computed in both the molecular plane and a plane perpendicular to the molecular plane for the Si_3C_5 and Si_4C_8 systems. These plots are in complete agreement with the ring current analysis. The σ-component clearly depicts paratropic regions at the center of the C_5 rings in both Si_3C_5 and Si_4C_8, in accord with the presence of paratropic ring currents inside these rings. In addition, an intense diatropic region (long-range) centered on the local Si-ptC-Si ring is observed supporting the presence of a local diatropic current in this region. The π-component exhibits a strong diatropic region around the whole Si_3C_5 and Si_4C_8 ring (long-range), in agreement with the presence of a global diatropic ring current. As indicated previously [62,91], the NICS analysis does not allow the identification of all the ring current circuits. However, it is a suitable complement to understand the magnetic behavior of these species and the interpretation of their aromaticity under the magnetic criterion. Figure 6 shows a classical $NICS_{zz}$ analysis, i.e., discrete measurements at the center of the ring and 1.0 A above. The values measured in the molecular plane are pretty large (presumably because of the coupling of bond contributions). In contrast, the values above the plane agree with the current strength values measured in the induced current density analysis. In addition, Figures S6-S8 show an identical $NICS_{zz}$ analysis for $Si_2C_5H_2$, the cyclopentadienyl anion ($C_5H_5^-$) and the pentalene dianion ($C_8H_6^{2-}$). As seen with the current density analysis, diatropicity due to π-delocalization decreases for species with ptCs, presumably by the electron cloud polarization towards silicon atoms.

Preprints (www.preprints.org) | NOT PEER-REVIEWED | Posted: 25 August 2021 doi:10.20944/preprints202108.0499.v1

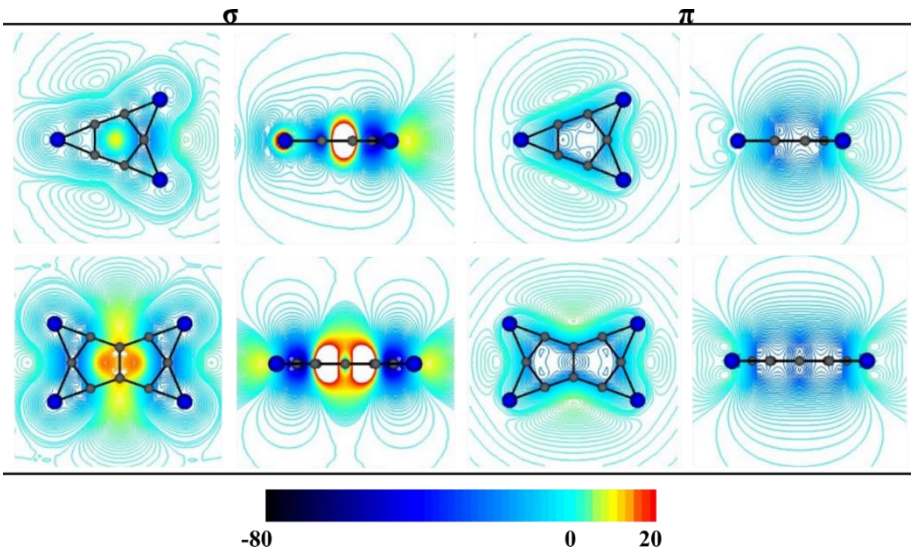

Figure 5. Isolines of the σ- and π-components of $NICS_{zz}$ for the studied molecules (at the GIAO-B3LYP/6-311+G*// B3LYP/6-311+G* level). The isolines are plotted in both the molecular plane (left) and a plane perpendicular to the molecular plane (right). The color scale at the bottom is in ppm.

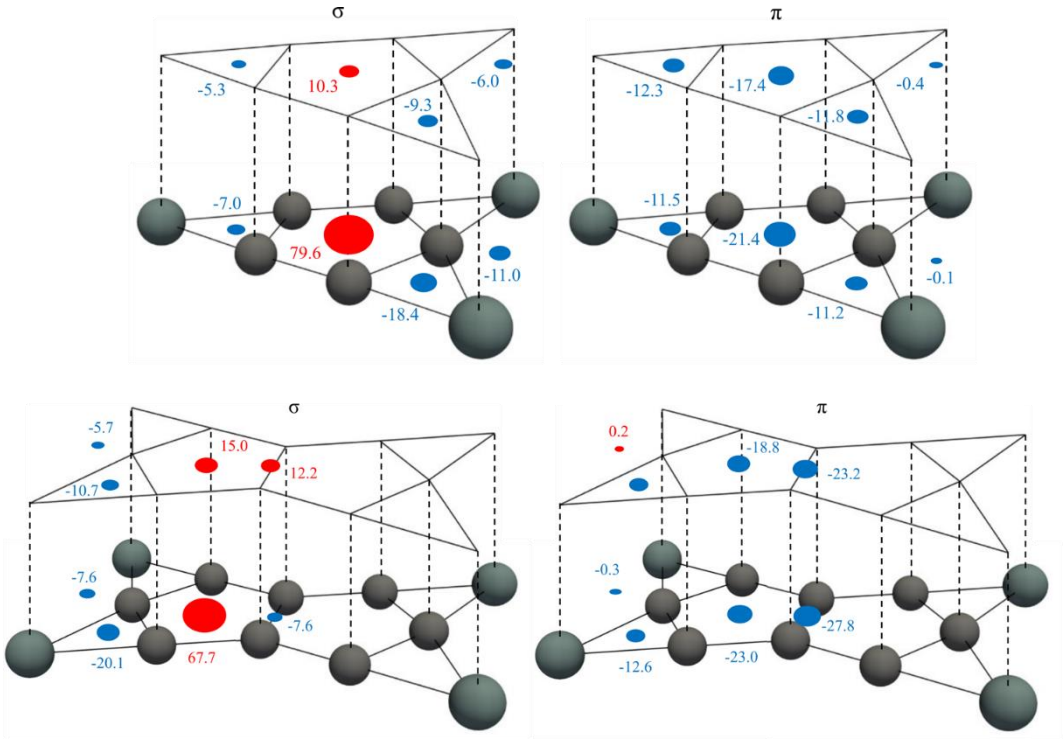

Figure 6. Computed values (in ppm) of σ- and π-components (left and right sides) of $NICS_{zz}$ at and above the ring centers (local and global) of studied molecules (at the GIAO-B3LYP/6-311+G*// B3LYP/6-311+G* level). The blue/red dots denote diatropic/paratropic character, and the dot size is in line with the $NICS_{zz}$ magnitude.

 doi:10.20944/preprints202108.0499.v1

4. Conclusions

The global (π) and local (σ) aromaticity of Si_3C_5 and Si_4C_8 clusters has been reviewed employing an orbital localization method (ELF-LOC) and magnetically induced current density analysis. The ELF-LOC investigation leads to bond descriptions similar to those reported previously based on the adaptive natural partitioning analysis (AdNDP) method. These systems show sigma and pi delocalization in agreement with Hückel's rule of 4n+2 electrons. The induced current density analysis identifies global and local aromatic current circuits. In the case of Si_3C_5, a local paratropic current (of moderate-intensity, RCS=-8.1 nA T^{-1}) is detected inside the C_5 ring. However, a diatropic current of higher intensity (RCS=12.16 nA T^{-1}) is also present, which provides a global aromatic character to this species. A local σ-diatropic current involving the Si-ptC-Si fragment is also identified, with moderate intensity (RCS=5.2 nA T^{-1}). These results highlight the double aromatic character of this species. In the case of Si_4C_8, a weak global paratropic current (RCS=-1.5 nA T^{-1}) and an intense global diatropic current (RCS=10.4 nA T^{-1}) are identified. In addition, two local diatropic currents around the Si-ptC-Si rings (RCS=5.8 nA T^{-1}) are also identified. This study highlights the double aromatic character of these clusters and the importance of this delocalization pattern in the stabilization of these species.

Supplementary Materials: The following are available online at www.mdpi.com/xxx/s1, **Table S1.** Cartesian coordinates of the studied systems, **Figure S1.** (a) Vector plot visualization of the current density of Si_3C_5 in a plane placed 0.5 Å above the molecular plane and top view of integration planes. (b) Integration profiles along the integration planes of Si_3C_5, **Figure S2.** (a) Vector plot visualization of the current density of Si_4C_8 in a plane placed 0.5 Å above the molecular plane and top view of integration planes. (b) Integration profiles along the integration planes of Si_4C_8, **Figure S3.** (a) Vector plot visualization of the current density of $C_5H_5^-$ in a plane placed 0.5 Å above the molecular plane and top view of integration planes (RCS are also reported in nA T^{-1}). (c) Integration profiles along the integration planes of $C_5H_5^-$, **Figure S4. (**a) Schematic representation of local and global currents. (b) Vector plot visualization of the current density of $C_8H_6^{2-}$ in a plane placed 0.5 Å above the molecular plane and top view of integration planes. (c) Integration profiles along the integration planes of $C_8H_6^{2-}$, **Figure S5.** (a) Schematic representation of local and global currents. (b) Vector plot visualization of the current density of $Si_2C_5H_2$ in a plane placed 0.5 Å above the molecular plane and top view of integration planes. (c) Integration profiles along the integration planes of $Si_2C_5H_2$, **Figure S6. (**a) Computed values (in ppm) of σ- and π-components (left and right sides) of $NICS_{zz}$ at and above the ring centers (local and global) of $Si_2C_5H_2$ (at the GIAO-B3LYP/6-311+G*// B3LYP/6-311+G* level). The blue/red dots denote diatropic/paratropic character, and the dot size is in line with the $NICS_{zz}$ magnitude. (b) Isolines of of the σ- and π-components of NICSzz for $Si_2C_5H_2$ (at the GIAO-B3LYP/6-311+G*// B3LYP/6-311+G* level). The isolines are plotted in both the molecular plane (left) and a plane perpendicular to the molecular plane (right). The color scale at the bottom is in ppm, **Figure S7.** Isolines of of the σ- and π-components of NICSzz for both the cyclopentadienyl anion ($C_5H_5^-$) and the pentalene dianion ($C_8H_6^{2-}$) (at the GIAO-B3LYP/6-311+G*// B3LYP/6-311+G* level). The isolines are plotted in both the molecular plane (left) and a plane perpendicular to the molecular plane (right). The color scale at the bottom is in ppm, **Figure S8.** Computed values (in ppm) of σ- and π-components (left and right sides) of $NICS_{zz}$ at and above the ring centers (local and global) of both the cyclopentadienyl anion ($C_5H_5^-$) and the pentalene dianion ($C_8H_6^{2-}$) (at the GIAO-B3LYP/6-311+G*// B3LYP/6-311+G* level). The blue/red dots denote diatropic/paratropic character, and the dot size is in line with the $NICS_{zz}$ magnitude.

Author Contributions: "Conceptualization, J.T-V., V.G. and W.T.; methodology, J.T-V., V.G., D.R.A, O.B.O. and R.B-G.; Computations, J.T-V., V.G., A.V-E., D.R.A., O.B.O. and R.B-G., ; validation, D.R.A., O.B.O., L.L. and A.T.; formal analysis, W.T., D.R.A, L.L. and A.T.; investigation, J.T-V., V.G., D.R.A and W.T.; resources, D.R.A., L.L. and W.T.; writing—original draft preparation, J.T-V, W.T. and D.R.A.; writing—review and editing, O.B.O., V.G. and L.L.; supervision, D.R.A and W.T.; project administration, V.G and W.T.; funding acquisition, D.R.A., O.B.O. and W.T. All authors have read and agreed to the published version of the manuscript.

Funding: This research was funded by FONDECYT, grant number 1211128.

Acknowledgments: We thank the financial support of National Agency for Research and Development (ANID) through FONDECYT project 1211128 (W.T.) R.B-G. acknowledge financial support of FONDECYT Postdoctorado 3210037. Powered@NLHPC: This research was partially supported by the supercomputing infrastructure of the NLHPC (ECM-02). D.R.A. acknowledges financial support from the Universidad de Buenos Aires (Grant No. 20020150100157BA), D.R.A. and O.B.O. acknowledge financial support from the Consejo Nacional de Investigaciones Científicas y Técnicas (Grant Nos. PIP 11220130100377CO and PIP 11220130100311CO), and the Agencia Nacional de Promoción Científica y Tecnológica (Grant No. PICT201-0381), Argentina.

Conflicts of Interest: The authors declare no conflict of interest.

References

1. von Schleyer, P.R.; Jiao, H. What is aromaticity? *Pure Appl. Chem.* **1996**, *68*, 209–218.
2. Minkin, V.I.; Glukhovtsev, M.N.; Simkin, B.Y. *Aromaticity and antiaromaticity*; John Wiley & Sons, Incorporated, 1994; ISBN 0471593826.
3. Krygowski, T.M.; Cyrański, M.K. Structural Aspects of Aromaticity. *Chem. Rev.* **2001**, *101*, 1385–1420, doi:10.1021/cr990326u.
4. Schleyer, P. von R. Introduction: aromaticity. *Chem. Rev.* **2001**, *101*, 1115–1118.
5. Boldyrev, A.I.; Wang, L.-S. All-Metal Aromaticity and Antiaromaticity. *Chem. Rev.* **2005**, *105*, 3716–3757, doi:10.1021/cr030091t.
6. Liu, C.; Popov, I.A.; Chen, Z.; Boldyrev, A.I.; Sun, Z. Aromaticity and antiaromaticity in Zintl clusters. *Chem. Eur. J.* **2018**, *24*, 14583–14597.
7. Boldyrev, A.I.; Wang, L.-S.S. Beyond organic chemistry: aromaticity in atomic clusters. *Phys. Chem. Chem. Phys.* **2016**, *18*, 11589–11605, doi:10.1039/c5cp07465g.
8. Alexandrova, A.N.; Boldyrev, A.I.; Zhai, H.-J.J.; Wang, L.-S.S. All-boron aromatic clusters as potential new inorganic ligands and building blocks in chemistry. *Coord. Chem. Rev.* **2006**, *250*, 2811–2866, doi:http://dx.doi.org/10.1016/j.ccr.2006.03.032.
9. Sergeeva, A.P.; Popov, I.A.; Piazza, Z.A.; Li, W.-L.; Romanescu, C.; Wang, L.-S.; Boldyrev, A.I. Understanding boron through size-selected clusters: structure, chemical bonding, and fluxionality. *Acc. Chem. Res.* **2014**, *47*, 1349–1358.
10. Mercero, J.M.; Boldyrev, A.I.; Merino, G.; Ugalde, J.M. Recent developments and future prospects of all-metal aromatic compounds. *Chem. Soc. Rev.* **2015**, *44*, 6519–6534.
11. Huang, X.; Zhai, H.; Kiran, B.; Wang, L. Observation of d-orbital aromaticity. *Angew. Chemie* **2005**, *117*, 7417–7420.
12. Tsipis, C.A. DFT study of "all-metal" aromatic compounds. *Coord. Chem. Rev.* **2005**, *249*, 2740–2762.
13. Rabanal-León, W.; Vásquez-Espinal, A.; Yañez, O.; Pino-Rios, R.; Arratia-Pérez, R.; Alvarez-Thon, L.; Torres-Vega, J.; Tiznado, W. Aromaticity of [M3 (μ-X) 3X6] 0/2-(M= Re and Tc, X= Cl, Br, I) Clusters Confirmed by Ring Current Analysis and Induced Magnetic Field. *Eur. J. Inorg. Chem.* **2018**, *2018*, 3312–3319.
14. Vásquez-Espinal, A.; Pino-Rios, R.; Alvarez-Thon, L.; Rabanal-León, W.A.; Torres-Vega, J.J.; Arratia-Perez, R.; Tiznado, W. New Insights into Re3 (μ-Cl) 3Cl6 Aromaticity. Evidence of σ-and π-Diatropicity. *J. Phys. Chem. Lett.* **2015**, *6*, 4326–4330.
15. Bleeke, J.R.; Behm, R.; Xie, Y.-F.; Chiang, M.Y.; Robinson, K.D.; Beatty, A.M. Synthesis, Structure, Spectroscopy, and Reactivity of a Metallabenzene1. *Organometallics* **1997**, *16*, 606–623.
16. Bleeke, J.R.; Xie, Y.F.; Peng, W.J.; Chiang, M. Metallabenzene: synthesis, structure, and spectroscopy of a 1-irida-3, 5-dimethylbenzene complex. *J. Am. Chem. Soc.* **1989**, *111*, 4118–4120.
17. Bleeke, J.R. Metallabenzenes. *Chem. Rev.* **2001**, *101*, 1205–1228.
18. Fernández, I.; Frenking, G.; Merino, G. Aromaticity of metallabenzenes and related compounds. *Chem. Soc. Rev.* **2015**, *44*, 6452–6463.
19. Vásquez-Espinal, A.; Poater, J.; Solà, M.; Tiznado, W.; Islas, R. Testing the effectiveness of the isoelectronic substitution principle through the transformation of aromatic osmathiophene derivatives into their inorganic analogues. *New J. Chem.* **2017**, *41*, 1168–1178.
20. Popov, I.A.; Bozhenko, K. V; Boldyrev, A.I. Is graphene aromatic? *Nano Res.* **2012**, *5*, 117–123.
21. Zubarev, D.Y.; Boldyrev, A.I. Revealing intuitively assessable chemical bonding patterns in organic aromatic molecules via adaptive natural density partitioning. *J. Org. Chem.* **2008**, *73*, 9251–9258.
22. Tkachenko, N. V; Boldyrev, A.I. Multiple local σ-aromaticity of nonagermanide clusters. *Chem. Sci.* **2019**, *10*, 5761–5765.
23. Hoffmann, R.; Alder, R.W.; Wilcox, C.F. Planar tetracoordinate carbon. *J. Am. Chem. Soc.* **1970**, *92*, 4992–4993, doi:10.1021/ja00719a044.
24. Erker, G. Planar-Tetracoordinate Carbon: Making Stable Anti-van' t Hoff/LeBel Compounds. *Comments Inorg. Chem.* **1992**, *13*, 111–131.
25. Röttger, D.; Erker, G. Compounds Containing Planar-Tetracoordinate Carbon. *Angew. Chemie Int. Ed. English* **1997**, *36*, 812–827.
26. Siebert, W.; Gunale, A. Compounds containing a planar-tetracoordinate carbon atom as analogues of planar methane. *Chem. Soc. Rev.* **1999**, *28*, 367–371.
27. Keese, R. Carbon flatland: planar tetracoordinate carbon and fenestranes. *Chem. Rev.* **2006**, *106*, 4787–4808.
28. Merino, G.; Méndez-Rojas, M.A.; Vela, A.; Heine, T. Recent advances in planar tetracoordinate carbon chemistry. *J. Comput. Chem.* **2007**, *28*, 362–372.

29. Zhang, X.; Ding, Y. Computational prediction of a global planar penta-coordinate carbon structure CAl4Ga+. *Comput. Theor. Chem.* **2014**, *1048*, 18–24.
30. Li, X.; Zhang, H.; Wang, L.; Geske, G.D.; Boldyrev, A.I. Pentaatomic tetracoordinate planar carbon,[CAl4] 2−: a new structural unit and its salt complexes. *Angew. Chemie Int. Ed.* **2000**, *39*, 3630–3632.
31. Wang, Z.-X.; von Ragué Schleyer, P. Construction principles of" hyparenes": families of molecules with planar pentacoordinate carbons. *Science (80-.).* **2001**, *292*, 2465–2469.
32. Wang, Y.; Li, F.; Li, Y.; Chen, Z. Semi-metallic Be 5 C 2 monolayer global minimum with quasi-planar pentacoordinate carbons and negative Poisson's ratio. *Nat. Commun.* **2016**, *7*, 11488.
33. Pan, S.; Cabellos, J.L.; Orozco-Ic, M.; Chattaraj, P.K.; Zhao, L.; Merino, G. Planar pentacoordinate carbon in CGa 5+ derivatives. *Phys. Chem. Chem. Phys.* **2018**, *20*, 12350–12355.
34. Pei, Y.; An, W.; Ito, K.; Schleyer, P. von R.; Zeng, X.C. Planar pentacoordinate carbon in CAl5+: a global minimum. *J. Am. Chem. Soc.* **2008**, *130*, 10394–10400.
35. Vassilev-Galindo, V.; Pan, S.; Donald, K.J.; Merino, G. Planar pentacoordinate carbons. *Nat. Rev. Chem.* **2018**, *2*, 114.
36. Grande-Aztatzi, R.; Cabellos, J.L.; Islas, R.; Infante, I.; Mercero, J.M.; Restrepo, A.; Merino, G. Planar pentacoordinate carbons in CBe 5 4− derivatives. *Phys. Chem. Chem. Phys.* **2015**, *17*, 4620–4624.
37. Zhao, X.-F.; Bian, J.-H.; Huang, F.; Yuan, C.; Wang, Q.; Liu, P.; Li, D.; Wang, X.; Wu, Y.-B. Stabilization of beryllium-containing planar pentacoordinate carbon species through attaching hydrogen atoms. *RSC Adv.* **2018**, *8*, 36521–36526.
38. Grande-Aztatzi, R.; Cabellos, J.L.; Islas, R.; Infante, I.; Mercero, J.M.; Restrepo, A.; Merino, G. Planar pentacoordinate carbons in CBe54− derivatives. *Phys. Chem. Chem. Phys.* **2015**, *17*, 4620–4624, doi:10.1039/C4CP05659K.
39. Cui, Z.; Vassilev-Galindo, V.; Cabellos, J.L.; Osorio, E.; Orozco, M.; Pan, S.; Ding, Y.; Merino, G. Planar pentacoordinate carbon atoms embedded in a metallocene framework. *Chem. Commun.* **2017**, *53*, 138–141.
40. Wu, Y.-B.; Duan, Y.; Lu, G.; Lu, H.-G.; Yang, P.; von Rague Schleyer, P.; Merino, G.; Islas, R.; Wang, Z.-X. D 3h CN 3 Be 3+ and CO 3 Li 3+: viable planar hexacoordinate carbon prototypes. *Phys. Chem. Chem. Phys.* **2012**, *14*, 14760–14763.
41. Exner, K.; von Ragué Schleyer, P. Planar hexacoordinate carbon: a viable possibility. *Science (80-.).* **2000**, *290*, 1937–1940.
42. Parra, L.L.; Diego, L.; Yañez, O.; Inostroza, D.; Barroso, J.; Espinal, A.V.; Merino, G.; Tiznado, W. Planar Hexacoordinate Carbons: Half Covalent, Half Ionic. *Angew. Chem. Int. Ed. Engl.* **2021**, *60*, 8700–8704.
43. Li, Y.; Liao, Y.; Chen, Z. Be2C monolayer with quasi-planar hexacoordinate carbons: a global minimum structure. *Angew. Chemie* **2014**, *126*, 7376–7380.
44. Feixas, F.; Matito, E.; Poater, J.; Sola, M. Quantifying aromaticity with electron delocalisation measures. *Chem. Soc. Rev.* **2015**, *44*, 6434–6451, doi:10.1039/C5CS00066A.
45. Gomes, J.; Mallion, R.B. Aromaticity and ring currents. *Chem. Rev.* **2001**, *101*, 1349–1384.
46. Mitchell, R.H. Measuring aromaticity by NMR. *Chem. Rev.* **2001**, *101*, 1301–1316.
47. Cyranski, M.K.; Krygowski, T.M.; Katritzky, A.R.; Schleyer, P. von R. To what extent can aromaticity be defined uniquely? *J. Org. Chem.* **2002**, *67*, 1333–1338.
48. Randic, M. Aromaticity of polycyclic conjugated hydrocarbons. *Chem. Rev.* **2003**, *103*, 3449–3606.
49. Balaban, A.T.; Oniciu, D.C.; Katritzky, A.R. Aromaticity as a cornerstone of heterocyclic chemistry. *Chem. Rev.* **2004**, *104*, 2777–2812.
50. McWeeny, R. Ring currents and proton magnetic resonance in aromatic molecules. *Mol. Phys.* **1958**, *1*, 311–321.
51. Pople, J.A. Molecular orbital theory of aromatic ring currents. *Mol. Phys.* **1958**, *1*, 175–180.
52. Pauling, L. The diamagnetic anisotropy of aromatic molecules. *J. Chem. Phys.* **1936**, *4*, 673–677.
53. Kumar, C.; Fliegl, H.; Sundholm, D. Relation Between Ring Currents and Hydrogenation Enthalpies for Assessing the Degree of Aromaticity. *J. Phys. Chem. A* **2017**, *121*, 7282–7289.
54. Ligabue, A.; Pincelli, U.; Lazzeretti, P.; Zanasi, R. Current density maps, magnetizability, and nuclear magnetic shielding tensors for anthracene, phenanthrene, and triphenylene. *J. Am. Chem. Soc.* **1999**, *121*, 5513–5518.
55. Monaco, G.; Fowler, P.W.; Lillington, M.; Zanasi, R. Designing paramagnetic circulenes. *Angew. Chemie* **2007**, *119*, 1921–1924.
56. Lazzeretti, P. Assessment of aromaticity via molecular response properties. *Phys. Chem. Chem. Phys.* **2004**, *6*, 217–223.
57. Schleyer, P. von R.; Maerker, C.; Dransfeld, A.; Jiao, H.; Hommes, N.J.R. van E. Nucleus-independent chemical shifts: a simple and efficient aromaticity probe. *J. Am. Chem. Soc.* **1996**, *118*, 6317–6318.
58. Haddon, R.C. The application of the Biot-Savart law to the ring current analysis of proton chemical shifts—II: An approach to aromatic character in the annulenes. *Tetrahedron* **1972**, *28*, 3635–3655.
59. Báez-Grez, R.; Rabanal-León, W.A.; Alvarez-Thon, L.; Ruiz, L.; Tiznado, W.; Pino-Rios, R. Aromaticity in heterocyclic analogues of benzene: Dissected NICS and current density analysis. *J. Phys. Org. Chem.* **2019**, *32*, e3823.
60. Báez-Grez, R.; Ruiz, L.; Pino-Rios, R.; Tiznado, W. Which NICS method is most consistent with ring current analysis? Assessment in simple monocycles. *RSC Adv.* **2018**, *8*, 13446–13453.
61. Poater, J.; Solà, M.; Viglione, R.G.; Zanasi, R. Local aromaticity of the six-membered rings in pyracylene. A difficult case for the NICS indicator of aromaticity. *J. Org. Chem.* **2004**, *69*, 7537–7542.
62. Sundholm, D.; Berger, R.J.F.; Fliegl, H. Analysis of the magnetically induced current density of molecules consisting of annelated aromatic and antiaromatic hydrocarbon rings. *Phys. Chem. Chem. Phys.* **2016**, *18*, 15934–15942.
63. Yañez, O.; Vásquez-Espinal, A.; Báez-Grez, R.; Rabanal-León, W.A.; Osorio, E.; Ruiz, L.; Tiznado, W. Carbon rings decorated with group 14 elements: new aromatic clusters containing planar tetracoordinate carbon. *New J. Chem.* **2019**, *43*, 6781–6785, doi:10.1039/C9NJ01022J.

64. Yañez, O.; Báez-Grez, R.; Garza, J.; Pan, S.; Barroso, J.; Vásquez-Espinal, A.; Merino, G.; Tiznado, W. Embedding a Planar Hypercoordinate Carbon Atom into a [4n+ 2] π-System. *ChemPhysChem* **2020**, *21*, 145–148.
65. Yañez, O.; Vásquez-Espinal, A.; Pino-Rios, R.; Ferraro, F.; Pan, S.; Osorio, E.; Merino, G.; Tiznado, W. Exploiting electronic strategies to stabilize a planar tetracoordinate carbon in cyclic aromatic hydrocarbons. *Chem. Commun.* **2017**, *53*, 12112–12115, doi:10.1039/C7CC06248F.
66. Becke, A.D. Becke's three parameter hybrid method using the LYP correlation functional. *J. Chem. Phys* **1993**, *98*, 5648–5652.
67. Ditchfield, R.; Hehre, W.J.; Pople, J.A. Self-consistent molecular-orbital methods. IX. An extended Gaussian-type basis for molecular-orbital studies of organic molecules. *J. Chem. Phys.* **1971**, *54*, 724–728.
68. Hehre, W.J.; Ditchfield, R.; Pople, J.A. Self—consistent molecular orbital methods. XII. Further extensions of Gaussian—type basis sets for use in molecular orbital studies of organic molecules. *J. Chem. Phys.* **1972**, *56*, 2257–2261.
69. Frisch, M.J.; Trucks, G.W.; Schlegel, H.B.; Scuseria, G.E.; Robb, M.A.; Cheeseman, J.R.; Scalmani, G.; Barone, V.; Petersson, G.A.; Nakatsuji, H.; et al. Gaussian 16, revisión C.01. *Gaussian 16, Revis. C.01, Gaussian, Inc., Wallingford CT* 2016.
70. Oña, O.B.; Alcoba, D.R.; Tiznado, W.; Torre, A.; Lain, L. An orbital localization criterion based on the topological analysis of the electron localization function. *Int. J. Quantum Chem.* **2013**, *113*, 1401–1408.
71. Oña, O.B.; Alcoba, D.R.; Torre, A.; Lain, L.; Torres-Vega, J.J.; Tiznado, W. Orbital Localization Criterion as a Complementary Tool in the Bonding Analysis by Means of Electron Localization Function: Study of the Sin(BH)5-n2- (n = 0–5) Clusters. *J. Phys. Chem. A* **2013**, *117*, 12953–12958, doi:10.1021/jp4081228.
72. Alcoba, D.R.; Oña, O.B.; Torre, A.; Lain, L.; Tiznado, W. An orbital localization criterion based on the topological analysis of the electron localization function at correlated level. *Int. J. Quantum Chem.* **2018**, 118(14) e2558.
73. Oña, O.B.; Torres-Vega, J.J.; Torre, A.; Lain, L.; Alcoba, D.R.; Vásquez-Espinal, A.; Tiznado, W. Chemical bonding analysis in boron clusters by means of localized orbitals according to the electron localization function topology. *Theor. Chem. Acc.* **2015**, *134*, 28.
74. Schmidt, M.W.; Baldridge, K.K.; Boatz, J.A.; Elbert, S.T.; Gordon, M.S.; Jensen, J.H.; Koseki, S.; Matsunaga, N.; Nguyen, K.A.; Su, S. General atomic and molecular electronic structure system. *J. Comput. Chem.* **1993**, *14*, 1347–1363.
75. Noury, S.; Krokidis, X.; Fuster, F.; Silvi, B. Computational tools for the electron localization function topological analysis. *Comput. Chem.* **1999**, *23*, 597–604.
76. Wolinski, K.; Hinton, J.F.; Pulay, P. Efficient implementation of the gauge-independent atomic orbital method for NMR chemical shift calculations. *J. Am. Chem. Soc.* **1990**, *112*, 8251–8260.
77. Bohmann, J.A.; Weinhold, F.; Farrar, T.C. Natural chemical shielding analysis of nuclear magnetic resonance shielding tensors from gauge-including atomic orbital calculations. *J. Chem. Phys.* **1997**, *107*, 1173–1184.
78. Glendening, E.D.; Badenhoop, J.K.; Reed, A.E.; Carpenter, J.E.; Bohmann, J.A.; Morales, C.M.; Landis, C.R.; Weinhold, F. Natural bond orbital analysis program: NBO 6.0. *Theor. Chem. Institute, Univ. Wisconsin, Madison, WI* **2013**.
79. Childs, H.; Brugger, E.; Whitlock, B.; Meredith, J.; Ahern, S.; Pugmire, D.; Biagas, K.; Miller, M.; Harrison, C.; Weber, G.H.; et al. VisIt: An End-User Tool For Visualizing and Analyzing Very Large Data. In *High Performance Visualization--Enabling Extreme-Scale Scientific Insight*; 2012; pp. 357–372.
80. Fliegl, H.; Taubert, S.; Lehtonen, O.; Sundholm, D. The gauge including magnetically induced current method. *Phys. Chem. Chem. Phys.* **2011**, *13*, 20500–20518.
81. Jusélius, J.; Sundholm, D.; Gauss, J. Calculation of current densities using gauge-including atomic orbitals. *J. Chem. Phys.* **2004**, *121*, 3952–3963, doi:10.1063/1.1773136.
82. Ahrens, J.; Geveci, B.; Law, C. Paraview: An end-user tool for large data visualization. *Vis. Handb.* **2005**, *717*.
83. Ayachit, U. *The ParaView Guide: A Parallel Visualization Application*; Kitware, Inc.: USA, 2015; ISBN 1930934300, 9781930934306.
84. Abramowitz, M. *Handbook of Mathematical Functions, With Formulas, Graphs, and Mathematical Tables,*; Dover Publications, Inc.: New York, NY, USA, 1974; ISBN 0486612724.
85. Sundholm, D.; Fliegl, H.; Berger, R.J.F. Calculations of magnetically induced current densities: theory and applications. *Wiley Interdiscip. Rev. Comput. Mol. Sci.* **2016**, *6*, 639–678.
86. Hückel, E. Quantentheoretische Beiträge zum Benzolproblem. *Zeitschrift für Phys.* **1931**, *70*, 204–286, doi:10.1007/BF01339530.
87. Hückel, E. Quanstentheoretische Beiträge zum Benzolproblem. *Zeitschrift für Phys.* **1931**, *72*, 310–337, doi:10.1007/BF01341953.
88. Hückel, E. Zur Quantentheorie der Doppelbindung. *Zeitschrift für Phys.* **1930**, *60*, 423–456, doi:10.1007/BF01341254.
89. Lazzeretti, P. Ring currents. *Prog. Nucl. Magn. Reson. Spectrosc.* **2000**, *36*, 1–88.
90. Juse, J.; Sundholm, D. Ab initio determination of the induced ring current in aromatic molecules. *Phys. Chem. Chem. Phys.* **1999**, *1*, 3429–3435.
91. Inostroza, D.; García, V.; Yañez, O.; Torres-Vega, J.J.; Vásquez-Espinal, A.; Pino-Rios, R.; Báez-Grez, R.; Tiznado, W. On the NICS limitations to predict local and global current pathways in polycyclic systems. *New J. Chem.* **2021**, *45*, 8345–8351.
92. Aihara, J. Circuit resonance energy: A key quantity that links energetic and magnetic criteria of aromaticity. *J. Am. Chem. Soc.* **2006**, *128*, 2873–2879.